Inactivation of Escherichia coli L-aspartate aminotransferase by (S)-4-Amino-4,5-dihydro-2-thiophenecarboxylic acid reveals "A tale of two mechanisms"

ARTICLE *in* BIOCHEMISTRY · OCTOBER 2007

Impact Factor: 3.02 · DOI: 10.1021/bi700663n · Source: PubMed

Inactivation of *Escherichia coli* L-Aspartate Aminotransferase by (*S*)-4-Amino-4,5-dihydro-2-thiophenecarboxylic Acid Reveals "A Tale of Two Mechanisms"[†,‡]

Dali Liu,[§] Edwin Pozharski,[||] Bryan W. Lepore,[§,⊥] Mengmeng Fu,[#] Richard B. Silverman,[#] Gregory A. Petsko,[§] and Dagmar Ringe*[,§]

Department of Biochemistry and Chemistry and Rosenstiel Basic Medical Sciences Research Center MS029, Brandeis University, Waltham, Massachusetts 02454-9110, Department of Chemistry, Department of Biochemistry, Molecular Biology, and Cell Biology and the Center for Drug Discovery and Chemical Biology, Northwestern University, Evanston, Illinois 60208-3113, and Department of Pharmaceutical Sciences, University of Maryland, Baltimore, Maryland 21201

Received April 9, 2007; Revised Manuscript Received June 22, 2007

ABSTRACT: As a mechanism-based inactivator of PLP-enzymes, (*S*)-4-amino-4,5-dihydro-2-thiophenecarboxylic acid (SADTA) was cocrystallized with *Escherichia coli* aspartate aminotransferase (L-AspAT) at a series of pH values ranging from 6 to 8. Five structural models with high resolution (1.4−1.85 Å) were obtained for L-AspAT−SADTA complexes at pH 6.0, 6.5, 7.0, 7.5, and 8.0. Electron densities of the models showed that two different adducts had formed in the active sites. One adduct was formed from SADTA covalently linked to pyridoxal 5′-phosphate (PLP) while the other adduct was formed with the inhibitor covalently linked to Lysine246,[1] the active site lysine. Moreover, there is a strong indication based on the electron densities that the occurrence of the two adducts is pH dependent. We conclude that SADTA inactivates L-AspAT via two different mechanisms based on the binding direction of the inactivator. Additionally, the structural models also show pH dependence of the protein structure itself, which provided detailed mechanistic implications for L-AspAT.

Mechanism-based inactivators have been studied as early as the 1970s (*1*, *2*). Since this category of inhibitors requires catalytic activity of the target enzymes to carry out inhibition, they can potentially provide great inhibition specificity such as desired in clinical applications. One example is a natural product called D-cycloserine, presently being used as an antimycobacterial drug (*3*). Moreover, due to the large amount of knowledge accumulated in chemical mechanisms of enzymatic catalysis, it would be relatively convenient to rationally design such inhibitors as potential drugs. In the 1980s, (*S*)-4-amino-4,5-dihydro-2-thiophenecarboxylic acid (SADTA) (*4*) and (*S*)-4-amino-4,5-dihydro-2-furancarboxylic acid (SADFA) (*5*) were designed and synthesized as mechanism-based inhibitors against γ-aminobutyric acid aminotransferase (GABA-AT), modeled on the structure of gabaculine, a natural product and irreversible inhibitor, i.e., inactivator, of the enzyme. In the central nervous system, GABA-AT is responsible for regulating the balance between the inhibitory neurotransmitter GABA and the excitatory one L-glutamate. Inhibitors like SADTA and SADFA are thus potential drugs to increase the GABA level in the central nervous system and treat neurological disorders, such as epilepsy, depression, schizophrenia, etc. (*6*−*8*).

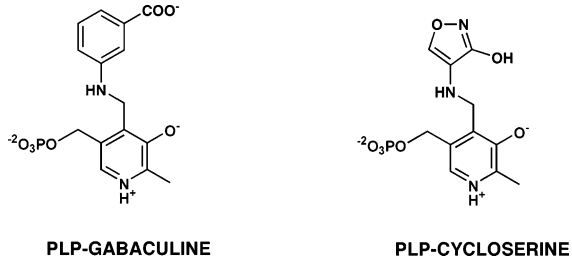

FIGURE 1: Previously reported PLP-inactivator adducts for D-cycloserine and gabaculine.

The mechanism of inactivation by gabaculine has been extensively studied. Three possible mechanisms were proposed (*9*). The data showed that gabaculine forms an irreversible adduct with PLP (Figure 1), the cofactor of GABA-AT (*10*−*12*), by a mechanism involving the ultimate aromatization of the ring. Besides gabaculine, cycloserine was also found to inactivate GABA-AT with the same aromatization mechanism (*13*) (Figure 1). Crystallographic studies conducted on cycloserine with D-amino acid aminotransferase (*14*) and alanine racemase, also PLP-dependent enzymes, provided concrete evidence on the aromatization mechanism (Figure 1) (*15*). This mechanism thus has become

[†] This research was supported by National Science Foundation Grant DBI 9874458 (to D.R.) and the National Institutes of Health Grant GM66132 (to R.B.S.).

[‡] The coordinates and structure factors of all five SADTA−L-aspartate aminotransferase complex structures have been deposited in the Protein Data Bank as entries 2Q7W, 2QA3, 2QB2, 2QB3, 2QBT.

* To whom correspondence should be addressed: Department of Biochemistry and Chemistry, and Rosenstiel Basic Sciences Research Center MS029, Brandeis University, PO Box 549110, Waltham, MA 02454-9110. Phone: 781-736-4902. Fax: 781-736-2405. E-mail: ringe@Brandeis.edu.

[§] Brandeis University.

[||] University of Maryland.

[⊥] Program in Bioorganic Chemistry.

[#] Northwestern University.

10.1021/bi700663n CCC: $37.00
Published on Web 08/22/2007 PAGE EST: 10.1

Scheme 1: Three Proposed Mechanisms for Inactivation of GABA Aminotranferase by SADTA/SADFA[a]

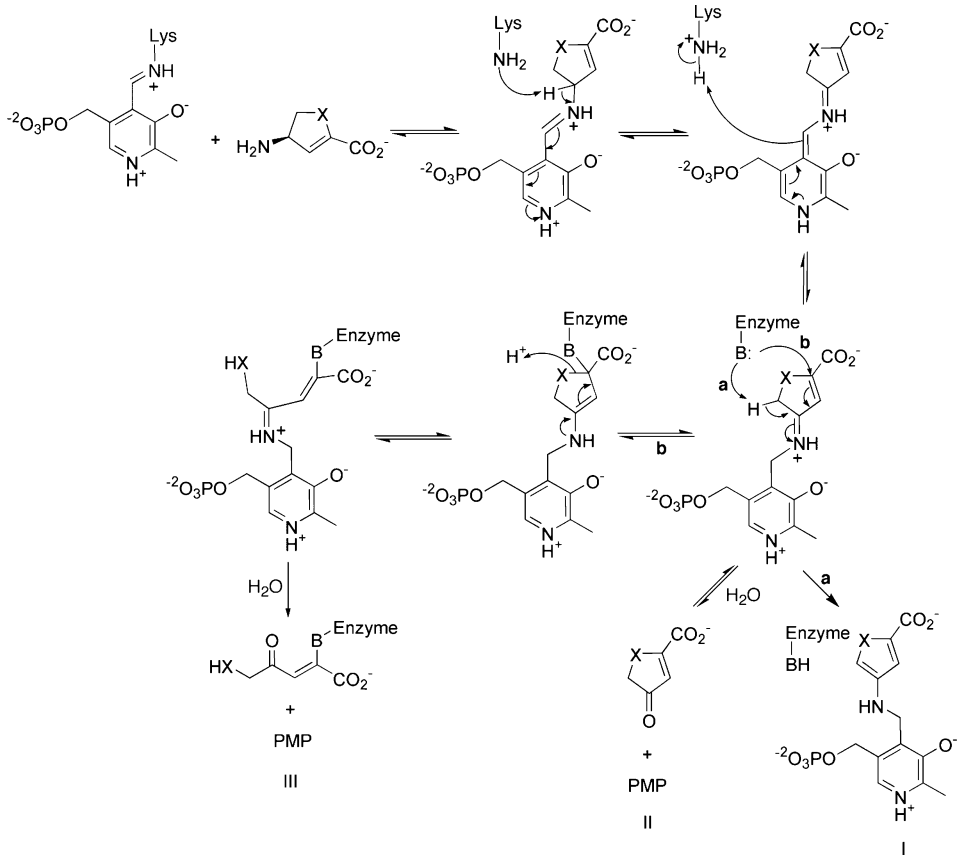

[a] Mechanism I leads to the formation of a PLP-inactivator adduct. Mechanism II is a side reaction producing a ketone product and PMP. Mechanism III is a ring-opening mechanism that forms an enzyme-inactivator adduct and PMP. a and b indicate the specific steps which lead to mechanisms I and III respectively. X stands for either a sulfur atom or an oxygen atom. B stands for a group from the enzyme that functions as a nucleophile in mechanism II or a general base in mechanism I.

the "generic" inactivation mechanism for cycloserine/gabaculine-like inhibitors.

Mechanistic studies with SADTA were also carried out against GABA-AT, and more than one inhibition mechanism was proposed (Scheme 1) (*16*, *17*). Besides the aromatization mechanism (Scheme 1, I), a ring-opening mechanism (Scheme 1, III) and a side reaction (Scheme 1, II) were also proposed, based on the detection of pyridoxamine 5′-phosphate (PMP) as a product from the inactivation of the enzyme. This unexpected result is reminiscent of the previous interpretation of the inactivation mechanism against GABA-AT (*9*), where the same types of mechanisms had been considered. Consequently, identification of the product of inactivation from structural evidence is needed to elucidate the true mechanisms of inactivation by SADTA.

Crystallography has been one of the most powerful tools to carry out mechanistic studies. Terms such as "structural enzymology" or "mechanistic crystallography" (*18*) have been used in this field. Obtaining the complex structures of inactivators with their target enzymes provides invaluable information on how exactly these potential drugs work. This would enhance endeavors of designing more effective drugs for new clinical treatments against, for instance, neurological disorders. However, the structure of the SADTA/GABA aminotransferase complex is not easy to obtain. As a mechanism-based process, inactivation by SADTA depends on the catalytic activity of the enzyme. Therefore, crystallization conditions must ensure that the catalytic activity is intact. Unfortunately, that is not the case for GABA aminotransferases because almost all known crystallization conditions for them are at relatively low pH values (3.0−6.0). At such pH values, the ϵ-amino group of the catalytic lysine, which is released after the formation of the external aldimine, would likely be protonated. Thus it cannot function as a general base to carry out the necessary catalytic steps that will eventually lead to formation of the final product of inactivation (Scheme 1). On the other hand, some similar PLP-dependent enzymes do crystallize at higher pH; aspartate aminotransferase from *E. coli* (L-AspAT) is known to crystallize at pH 7.4. Since L-AspAT catalyzes a very similar transamination reaction to GABA aminotransferases, it would be an excellent alternative model to carry out studies in elucidating the SADTA inactivation mechanism(s).

There are other intriguing reasons to use L-AspAT as an alternative model for this study. The mammalian aspartate aminotransferases, which are extremely similar to the *E. coli* L-AspAT in terms of both mechanism and structure, catalyze crucial reactions that are involved in the global metabolisms of the two neurotransmitters (L-glutamate and GABA) in the central nervous system (*19*−*23*) as well as other important metabolic pathways. For the purpose of designing drugs to cure neurological diseases, the effect of any drug against aspartate aminotransferase activity has to be taken into account. For example, gabaculine, which is too toxic to be used in clinical practice, has been found to have inhibitory effects on other PLP-dependent enzymes including aspartate

aminotransferase (*24*). Moreover, aspartate aminotransferase is one of the best studied PLP dependent enzymes. There are detailed mechanistic and structural studies on this enzyme dating from decades ago to recently (*25*−*31*). These provide a good foundation for us to investigate the detailed inhibition mechanisms of our inhibitors of interest once we are able to solve the complex structures. Alternatively, studies on the inhibition mechanisms also provide us a potential means to further look into the mechanistic details of the aspartate aminotransferase reaction.

In this paper, we present the structures of several complexes between SADTA and L-AspAT. Our efforts were extended into the realm of structural enzymology by exploiting the pH dependence of the inactivation by SADTA. More than one inactivation mechanism was revealed, producing two different end products, one involving derivatization of the cofactor, the other the active site lysine 246. (Traditionally, the numbering system of L-AspAT is not the real numbering for the protein but has been correlated to cytosolic aspartate aminotransferase based on sequence alignment. We decided to use the numbering solely based on the amino acid sequence of L-AspAT in this paper. For example, the catalytic lysine is labeled as K246 instead of K258, and two substrate-binding arginines are labeled as R374 and R280* instead of R386 and R292*.)

MATERIALS AND METHODS

Chemicals and Materials. Mechanism-based inactivator SADTA was synthesized according to reported methods (*4*). All other chemicals and enzymes used were purchased form Sigma-Aldrich/Fluka at the highest grade available.

Protein Preparation. The pJO2 plasmid (a gift kindly provided by Dr. J. F. Kirsch) containing the wild type *aspC* gene was transformed into the DH5α *E coli* strain. The wild type L-AspAT was overexpressed and purified with the protocol used by Onuffer and Kirsch (*32*). Accordingly, 0.1% of PLP was added to the expression culture. After breaking the harvested cells via sonication, the protein was first precipitated with 20% PEG8000. The protein was then redissolved and run through a DEAE column and a hydroxyapatite column on FPLC consecutively. The final yield of the purified L-AspAT is 80−100 mg/L of culture. For crystallizations at different pH values, the purified protein at 10 mg/mL was exchanged into 25 mM potassium phosphate buffer at pH 6.0, 6.5, 7.0, 7.5, 8.0, and 8.5 with final concentrations of 10 mg/mL. One millimolar PLP was supplemented to the protein solution to stabilize the enzyme.

Activity Assay and Inactivation Test. During and after the purification process, the activity of the aspartate aminotransferase was assayed via coupled reactions with lactate dehydrogenase and malate dehydrogenase according to Amador and Wacker (*33*). A typical assay reaction contains 100 mM sodium phosphate buffer (pH 7.4), 150 mM L-aspartate, 50 mM 2-oxoglutarate, 0.2 mM NADH, 40 units of lactate dehydrogenase, and 20 units of malate dehydrogenase. The reaction was initiated by adding 200 ng of purified L-AspAT, and the activity was measured using the spectrophotometric monitoring of the disappearance of NADH absorbance at 340 nm. To confirm the inactivation caused by SADTA, the aspartate aminotransferase (1 mg/mL) was preincubated with both 5 mM and 1 mM of inhibitor at room temperature and pH 7.4 for different periods of time before the remaining enzymatic activity was measured.

Crystallization. The cocrystallization of L-AspAT and SADTA was conducted using the hanging-drop method. The well solutions contained 25 mM potassium phosphate and 43% saturated ammonium sulfate. Hanging drops were set up by mixing 3 μL of protein solution (10 mg/mL), 1 μL of SADTA solution (100 mM), and 2 μL of well solution. The pH values of the solutions used had been adjusted to the desired values as indicated previously before mixing. The crystals appeared overnight. Crystals were then transferred to a cryo-protectant solution consisting of 48% saturated ammonium sulfate, 25 mM potassium phosphate, 20% glycerol, and 1 mM PLP, adjusted to the pH value at which the crystals were formed. The crystals were frozen in liquid nitrogen after dipping into cryo-protectant solutions.

Data Processing and Model Refinement. Monochromatic data sets were collected at a wavelength of 0.9 Å using a Quantum 315 CCD detector at station 14-BMC BioCars at the Advanced Photon Source, Argonne National Lab, and processed with the HKL2000 program suite (*34*). A known structural model for wild type *E. coli* aspartate aminotransferase (1AMQ) (*35*) was chosen as the initial model to conduct molecular replacement in CNS (*36*). After the solution was obtained, density fitting and model building were conducted via the program COOT (*37*). Simulated annealing and maximum likelihood model refinement on the improved structural models were carried out in CNS. Once the R_{free} decreased to around 30%, REFMAC5 (*38*) in the CCP4 program suite was then used to further refine the structural models via restrained refinement with isotropic or anisotropic *B* factors. When R_{free} stopped improving after a few rounds of refinement in REFMAC5, weight factors for restraints in restrained refinement (both isotropic and anisotropic) were increased till the lowest R_{free} was achieved for the refined model (Table 1).

All structure figures were made by using the POVSCRIPT+ program (*39*) (www.stanford/∼fenn/povscript), which is an extended version of molscript, and PYMOL program (http://www.pymol.org). The electron density maps shown in this paper were first generated with the FastFourierTransfer program in the CCP4 suite. Program MAPMAN from Uppsala Software Factory (http://xray.bmc.uu.se/usf) was then used to convert the maps from CCP4 format to O-map format so they can be read and displayed by POVSCRIPT+. Final figures were rendered by POVRAY (www.povray.org).

RESULTS

Inhibition of Enzymatic Activity by SADTA. Inhibition of L-AspAT by SADTA is both time and dose dependent. The course of inhibition was determined by activity assays after preincubating the enzyme in solution with two concentrations of SADTA (Figure 2). When assayed after 1.5 h of such preincubation, L-AspAT (1 mg/mL) treated with SADTA at 5 mM has only 17% activity remaining compared to the untreated enzyme. After preincubation for 12 h, the activity was almost completely gone, as only traces of activity (<3%) could be detected. On the other hand, when 1 mM SADTA was used, the activity cannot be inhibited completely even

Table 1: Crystallographic Statistics[a]

pdb code/pH value	2Q7W/6.0	2QA3/6.5	2QB2/7.0	2QB3/7.5	2QBT/8.0
resolution range, Å	28.9−1.40	27.0−1.75	27.0−1.70	24.8−1.45	24.8−1.75
space group	*C*2221	*C*2221	*C*2221	*C*2221	*C*2221
cell dimensions					
a, Å	153.6	153.9	153.9	153.3	154.1
b, Å	85.1	84.9	84.7	85.1	84.8
c, Å	78.8	78.9	78.9	78.8	79.0
total reflections	557011	360466	245032	578720	241679
unique reflections	98239	51173	54569	169762	48869
redundancy	5.7 (5.4)	7.0 (6.9)	4.5 (4.1)	6.5 (6.3)	4.7 (4.6)
completeness, %	96.4 (99.8)	99.6 (100)	96.1 (96.6)	97.1 (97.3)	98.2 (99.5)
linear R_{merge}, %	6.2 (57.1)	6.5 (56.6)	5.7 (52.5)	5.6 (51.6)	6.5 (58.9)
$I/\sigma(I)$	17.4 (2.7)	10.8 (3.3)	13.7 (2.6)	14.5 (3.6)	12.5 (2.3)
R_{crys}/R_{free}, %	15.6/18.8	15.7/19.7	14.7/18.4	14.4/17.8	16.1/19.4
rmsd bond, Å	0.02	0.01	0.02	0.02	0.01
rmsd angle, deg	1.9	1.4	1.8	1.9	1.5
average *B*, Å^2	23	22	22	23	24
disordered region	11−27	11−16, 24−27	9−16, 24−27	10−16, 20−27	none

[a] rmsd, root-mean-square deviation. Linear $R_{merge} = \sum|I_{obs} - I_{avg}|/\sum I_{avg}$. $R_{free} = \sum|F_{obs} - F_{calc}|/\sum F_{obs}$. Five percent of the reflection data were selected at random as test set and used to calculate R_{free}. R_{crys} was calculated with the same equation as R_{free}, but both test and working sets were used in the calculation. Numbers in parentheses are statistics for the highest resolution bin, whose ranges are 1.45−1.40 Å, 1.81−1.75 Å, 1.76−1.70 Å, 1.50−1.45 Å, and 1.81−1.75 Å, respectively.

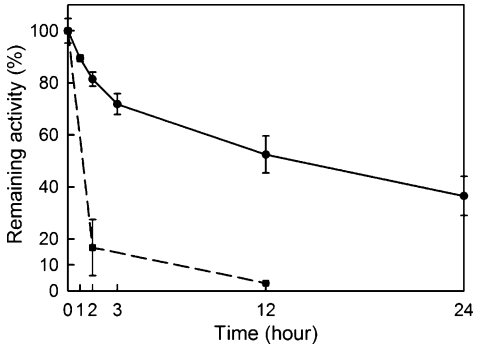

FIGURE 2: Inactivation of the L-AspAT activity by SADTA. The inactivation was measured as remaining activity after the enzyme had been treated with SADTA for various time periods. The dashed line represents the inhibition over time when 5 mM SADTA had been used to treat the enzyme prior to the activity assay. The solid line represents the inhibition over time when 1 mM SADTA had been used.

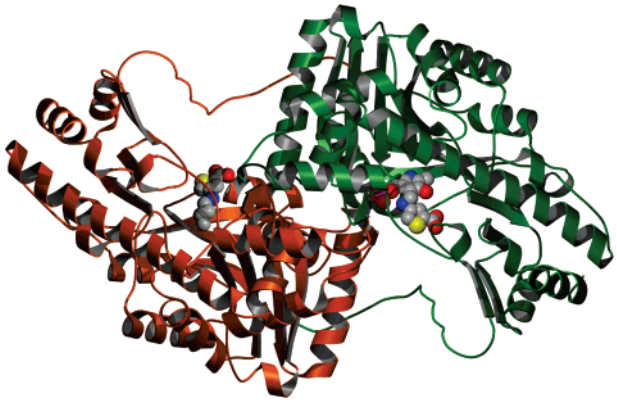

FIGURE 3: The structure of the L-AspAT dimer at pH 8.0. The dimeric structure was generated by applying a symmetry operator to one monomer. One monomer is in green while the other is in red. The two adducts formed, the PLP−SADTA adduct and the K246−SADTA adduct, are shown in space filled form representing the positions of two active sites respectively.

after 24 h of treatment. Removal of inhibitor via dilution of the pretreated enzyme 2500-fold with buffer did not restore activity, indicating irreversible inhibition/inactivation.

Crystallization and Data Collection. Crystals from co-crystallization of L-AspAT and SADTA appeared overnight at pH values of 6.0, 6.5, 7.0, 7.5, and 8.0, while none were obtained at pH 8.5. All crystals appear colorless in the presence of the inactivator, indicating loss of the conjugated aldimine linkage. Suitable single crystals (0.3−0.4 mm in the smallest dimension) were selected for data collection. The selected crystals diffracted to high resolutions ranging from 1.3 to 1.8 Å. The resolution cutoff during the process was made according to three criteria: (1) the value of R_{merge} of the highest resolution bin is less than 70%; (2) the value of $I/\sigma(I)$ of the highest resolution bin is no less than 2; (3) the completeness of the highest resolution bin is higher than 90%. All data sets were integrated and scaled using the HKL2000 program suite and had a total R_{merge} <10% (Table 1).

Overall Structural Models and Disordered Regions. All structures obtained here have the same overall structural features as those previously known. The enzyme can be delineated as an alpha/beta protein (Figure 3). Even though L-AspAT is a dimer, the structural models are first obtained as a monomer because two subunits in the same dimer are also crystallographically related to each other in the space group *C*2221. The coordinates of the other subunit in the dimer were generated by applying a symmetry operation (x, $-y$, $-z$) to the one obtained. All models presented in this paper have inactivator covalently bound at the active sites of the protein.

In models at pH 7.5 or lower a region from residues 9−27 in sequence was not observed in the electron density and is thus considered disordered. This region was truncated either fully or partially from those models (Table 1). This disordered region has relatively high *B* factor values in the models available in the PDB as well. For example, the initial model (1AMQ) (*35*) used for molecular replacement, determined at pH 7, shows *B* factor values of 70−80 Å^2 for most atoms in that region. Only at pH 8.0 does this region become ordered enough to be built as a helix. This region is part of the long "tail" that reaches over from one subunit to the other in the dimer and may be flexible enough to accommodate the relative movements of the two subunits. It is possible

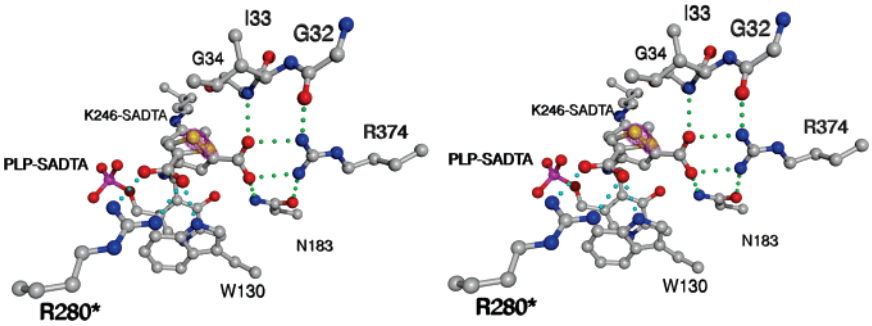

FIGURE 4: Stereo image of the two different adducts formed in the active site. The structure model at pH 7.5 was used in this figure to show the positions of the two adducts. Both adducts and amino acid residues in the active site are shown in ball-and-stick form. Only one of the two alternative conformations was shown for residues G32, I33, G34, and R280* for clarity. A PMP molecule which overlaps with the PLP moiety was also omitted from the figure. Carbon atoms are in gray color; nitrogen atoms are in blue; oxygen atoms are in red; the phosphorus atom of the PLP moiety is in magenta; two sulfur atoms in two adducts are shown in yellow surrounded by magenta mesh representing the $2F_o - F_c$ electron density map contoured at 4.5σ. The salt bridge and hydrogen bonds that contribute to binding the inactivator moiety in the PLP−SADTA adduct are shown as green dashed lines, while those contributing to binding the inactivator moiety in the K246−SADTA adduct are shown as cyan dashed lines.

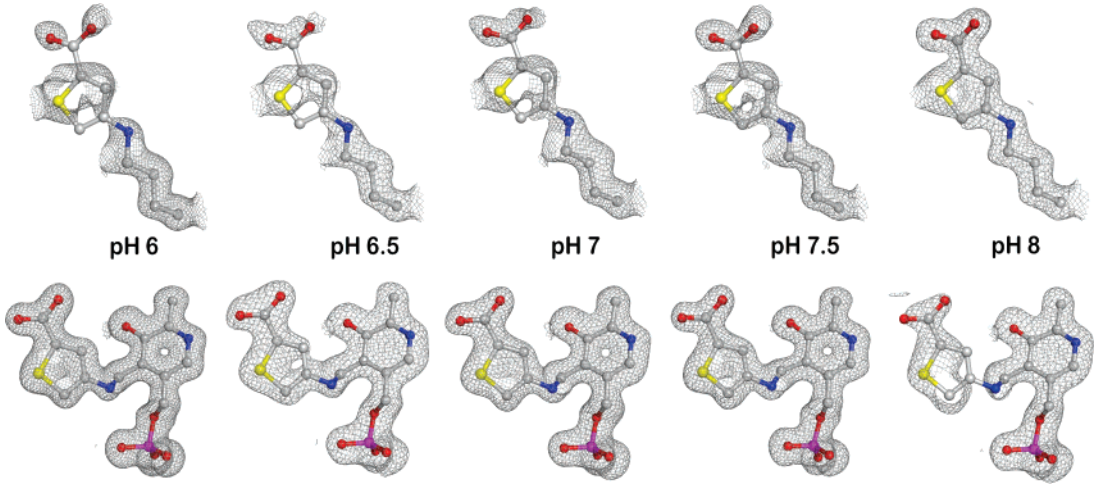

FIGURE 5: Electron density for adducts shows pH dependency. The top row shows only the K246−SADTA adducts and surrounding electron density, while the bottom row shows only the PLP−SADTA adducts and surrounding electron density from pH 6 to 8. The structural features other than the adducts were omitted for clarity. All adducts are shown in ball and stick form with oxygen atoms in red, carbon atoms in gray, nitrogen atoms in blue, and sulfur atoms in yellow. The $2F_o - F_c$ electron density maps contoured at 1σ are shown as gray meshes. The electron densities of two adducts at the same pH values are shown in the same column.

that the stability of the secondary structure in this region is pH dependent.

Identification of Two Different Adducts in the Same Active Site. In all structural models presented in this paper, two different adducts were built at the active sites based upon the electron density maps such as that shown (Figures 4 and 5). In one adduct, the inactivator is covalently bound to PLP (PLP−SADTA adduct) resulting in a free lysine 246 side chain. In addition, the nitrogen atom that connects the C4 atom of the thiophene ring to the PLP moiety is out of the PLP plane pointing away from the catalytic lysine. In the other adduct, the inactivator is covalently bound to the side chain of lysine 246 (K246−SADTA adduct). The formation of the K246−SADTA adduct results in 1 equiv of PMP, which is almost completely overlapped with the PLP moiety of the PLP−SADTA adduct. (The PMP was omitted in Figures 4, 5, and 6 for clarity, but it was shown in Figure 7 schematically.)

According to the electron density maps shown for the active sites, both adducts only occupy the active sites partially. The PLP−SADTA adduct is the dominant species in crystals formed at pH 6, while the K246−SADTA adduct is the dominant species in crystals formed at pH 8 (Figure 5). In either case, the newly formed covalent bond was convincingly supported by the continuity of the electron density between the inactivator and PLP or lysine 246. Leaving out either adduct from any structural model resulted in the appearance of positive difference ($F_o - F_c$) density that resembles the structural features of the missing adduct. Moreover, when an electron density ($2F_o - F_c$) map is contoured at a higher sigma level ($>4.5\sigma$) so that only density around sulfur atoms can be observed, the electron density shows dual sulfur positions, one from each adduct. Such an example is shown in Figure 4 with the structural model obtained from crystallization at pH 7.5. The same observations were made with all models presented.

The positions of the two adducts correlate well with the known specificity of the L-AspAT active site (Figures 4 and 7). In the PLP−SADTA adduct, the carboxylate group of the thiophene carboxylic acid moiety forms a salt bridge with the guanidinium group of arginine 374. In the K246−SADTA adduct, the carboxyl group of the inhibitor forms a salt bridge with the guanidinium group of arginine 280* from the other monomer.[2] Residues R374 and R280* constitute

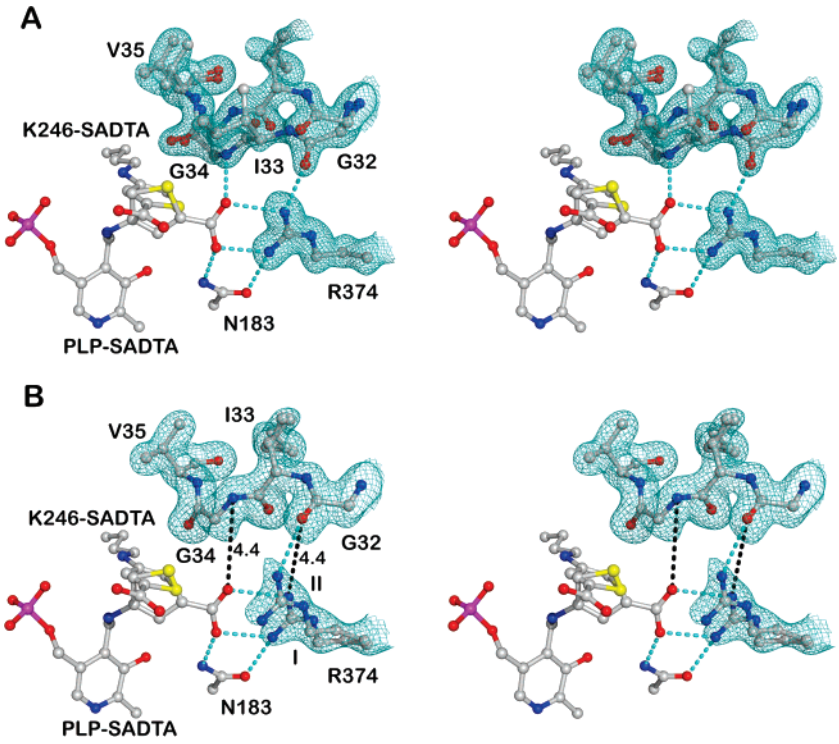

FIGURE 6: Stereo image of a region (residues 32−35) near the active site. The PLP−SADTA adduct, the K246−SADTA adduct, and the residues from 32 to 35 are shown along with some key binding residues in stick and ball form. The PMP molecule and the freed K246 sided chain were omitted for clarity. Structural model A was obtained at pH 6 while structural model B was obtained at pH 8. The cyan dashed line represents the interactions (hydrogen bonds and a salt bridge) contributed to the binding of inactivator carboxylate group. The black dashed line represents two hydrogen bonds that were broken due to the movement of the loop region (residues 32−35), labeled with the measurements of the distances in angstroms. In the structural model A, residues 32−35 are built in two different alternate conformers resulting in the dual position of this stretch of backbone. In structural model B two alternative conformations for the R374 side chain are labeled as I and II. The electron density map ($2F_o - F_c$ map contoured at the 1σ level) around the residues 32−35 along with R374 is shown as cyan mesh.

the binding sites for the dicarboxylic acid substrates in the native catalytic reaction: the main chain carboxylate of aspartate interacts with R374, the side chain carboxylate interacts with R280*. Such correlation thus strongly supports the fact that SADTA can take advantage of the L-AspAT binding sites differently to form the two adducts observed. Besides the salt bridges mentioned above, N183, G32, and G34 all contribute to the binding of the PLP−SADTA adduct by forming a hydrogen-bonding network with the carboxylate of the SADTA moiety (Figures 4, 6, and 7). Meanwhile, W130 forms a hydrogen bond between its side chain nitrogen and one of the carboxylate oxygen atoms of the K246−SADTA adduct.

The two adducts overlap with each other such that the thiophene rings of the two adducts are in two planes that are almost perpendicular to each other (Figure 4). Such an arrangement makes the true "coexistence" of the two adducts in the same active site impossible. Therefore, all the structural models presented in this paper are actually the average structural models of two species existing in the same crystal. No electron density was observed to provide evidence for the existence of the internal aldimine of PLP, meaning that all active protein molecules in the crystal reacted with the inactivator one way or the other.

The Nature of the Adduct is pH Dependent. The overall changes in occupancy and electron density clearly show that the occurrence of the two adducts is pH dependent (Figure 5). At pH 6, the electron density suggests the dominating adduct species to be PLP−SADTA. Only traces of electron density can be observed around the position of the K246−SADTA adduct. With an increase in pH value of the crystallization conditions, electron density features around the K246−SADTA adduct position show the presence of this adduct. When the pH value is at its highest (pH 8), the dominating species is clearly the K246−SADTA adduct. While the height of the electron density correlating with the PLP−SADTA adduct does not change dramatically from pH 6 to 7.5, it fades away at pH 8 so that contiguous electron density (at 1σ level) is no longer present to account for this adduct.

Estimation of the Occupancies of Two Different Adducts. Because the two proposed adducts cannot coexist in the same active site, and because there is no evidence for an internal aldimine, the total occupancy was set to 1. A crude estimation of the individual occupancies of both adducts was conducted manually. Carbon 3 of the thiophene ring is an atom that does not overlap in the two adducts and is in a very similar chemical environment in either one. Therefore, the heights of the electron density peaks ($2F_o - F_c$ map) around the C3 position in either adduct were measured using the program COOT (*37*). The occupancies of the two adducts were estimated based on the ratio of the measured peak heights relative to those of their own C3 positions. Moreover, the alternate conformers of the residues that are directly involved in forming these adducts, including K246 and PMP, were

[1] The residues labeled with an ∗ belong to the other subunit of the physiological dimer of this L-AspAT.

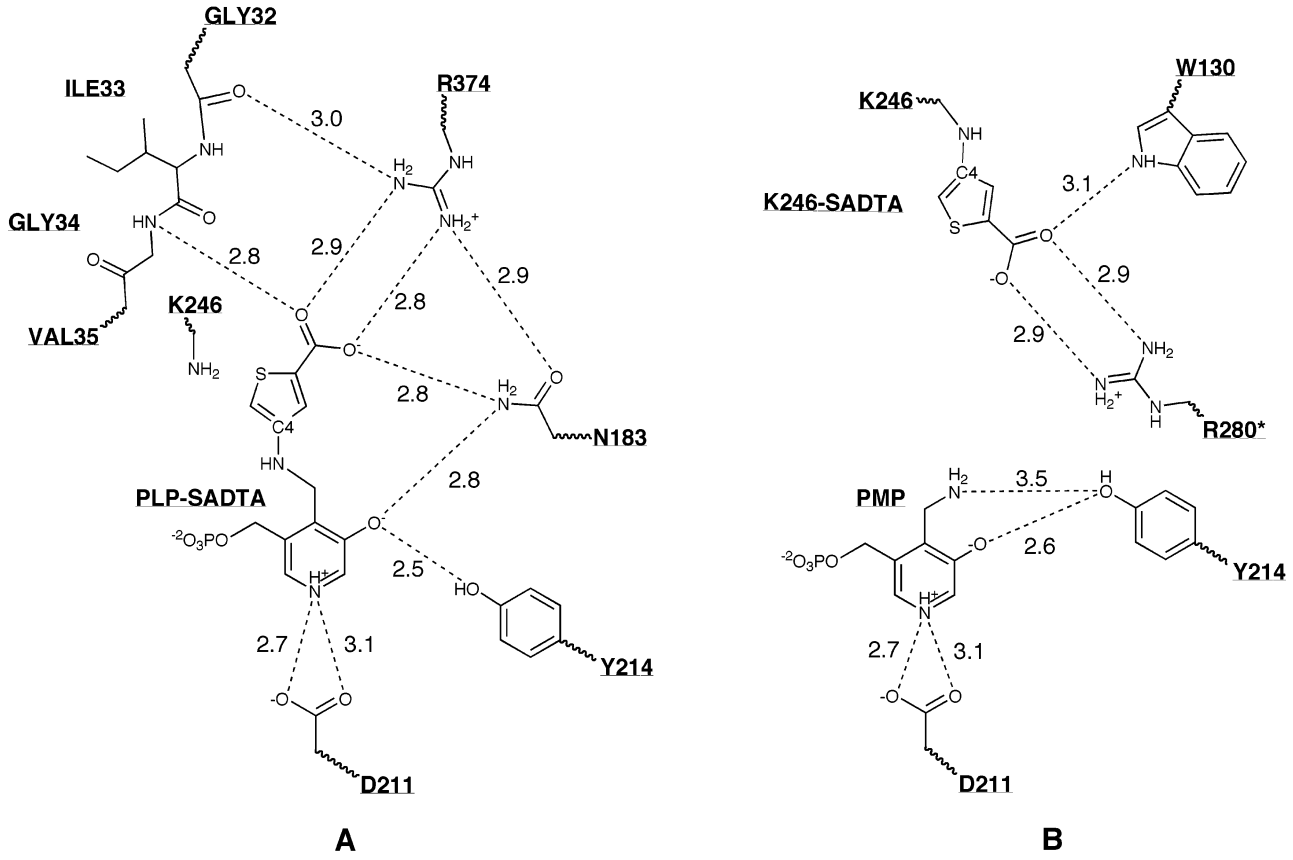

FIGURE 7: Schematic diagrams of the two different adducts in the active site of L-AspAT. The key distances are indicated with dashed lines and labeled with numbers in angstroms. All distances were measured in the structure model obtained at pH 7.5. The name and number of the amino acid residues involved are shown underlined. The "C4" is the carbon 4 atom in the thiophene ring. (A) Interactions of the PLP−SADTA adduct in the active site. (B) Interactions of the K246−SADTA adduct in the active site.

built with the same occupancies as the corresponding adducts. The estimated occupancies were included in the next round of refinement to generate a structural model. The whole process was repeated until no further adjustment was needed. The occupancies estimated for K246−SADTA are 30% (pH 6), 35% (pH 6.5), 35% (pH 7), 40% (pH 7.5), and 75% (pH 8) with the PLP−SADTA accounting for the difference.

Alternate Conformers in the Structure Models. In all models presented, there are a number of residues built with alternate conformers. These are expected due to the high resolutions achieved, the different pH's at which the structures were obtained, and the fact that each crystal is composed of protein molecules with two types of inhibitor adducts.

Residues 32−35 of the active site were reported as part of a hydrophobic lid at the entrance of the substrate binding pocket, with conformational changes associated with substrate binding (*15*, *31*, *40*). The peptide backbone of these residues takes on two alternative configurations in models obtained at pH 7.5 or lower (Figure 6A). Their occupancies were refined to approximately 50%. At pH 8 only one configuration is observed, in a direction away from bound ligand (Figure 6B). However, at this pH two configurations of the R374 side chain are observed (occupancies refined to approximately 50%). The occupancies of the alternate conformers in this region are not correlated to the adduct occupancies in the same model, but do seem to be correlated to the changes in pH between models. These alternate conformations have profound effects on the interactions between the PLP−SADTA adduct and the protein.

In all models, the carboxylate group of the PLP−SADTA adduct forms a bidentate salt bridge with the guanidinium group of R374. However, the interactions between the atoms of this salt bridge and the protein change in a pH dependent manner (Figure 6). In the structural models obtained at pH 7.5 or lower (Figure 6A), in addition to the salt bridge interactions, one oxygen atom of the carboxylate group of the PLP−SADTA adduct interacts with the backbone nitrogen of G34, and one nitrogen of the guanidinium group interacts with the backbone carbonyl group of G32, in one of the conformations (closer) observed for the backbone. These interactions are ideal to stabilize the position of the adduct in the protein. In the other conformation of this region, the away conformation, these interactions are lost.

In the structural models obtained at pH 8 (Figure 6B), only one backbone conformation is observed. This conformation corresponds to the away conformation at pH 7.5 or lower, in which the salt bridge makes no interactions with the protein (distances greater than 4 Å). However, an alternate conformation for R374 (conformation II) is observed that does retain an interaction with the carbonyl group of G32. In this conformation the salt bridge between the carboxylate of the adduct and the side chain of R374 is retained (distance 3.1 Å) but with less ideal interaction distances, and the carbonyl oxygen interaction with G34 is not observed. With either conformation of R374, the interactions between adduct

Scheme 2: Proposed Inactivation Mechanisms of L-AspAT by SADTA[a]

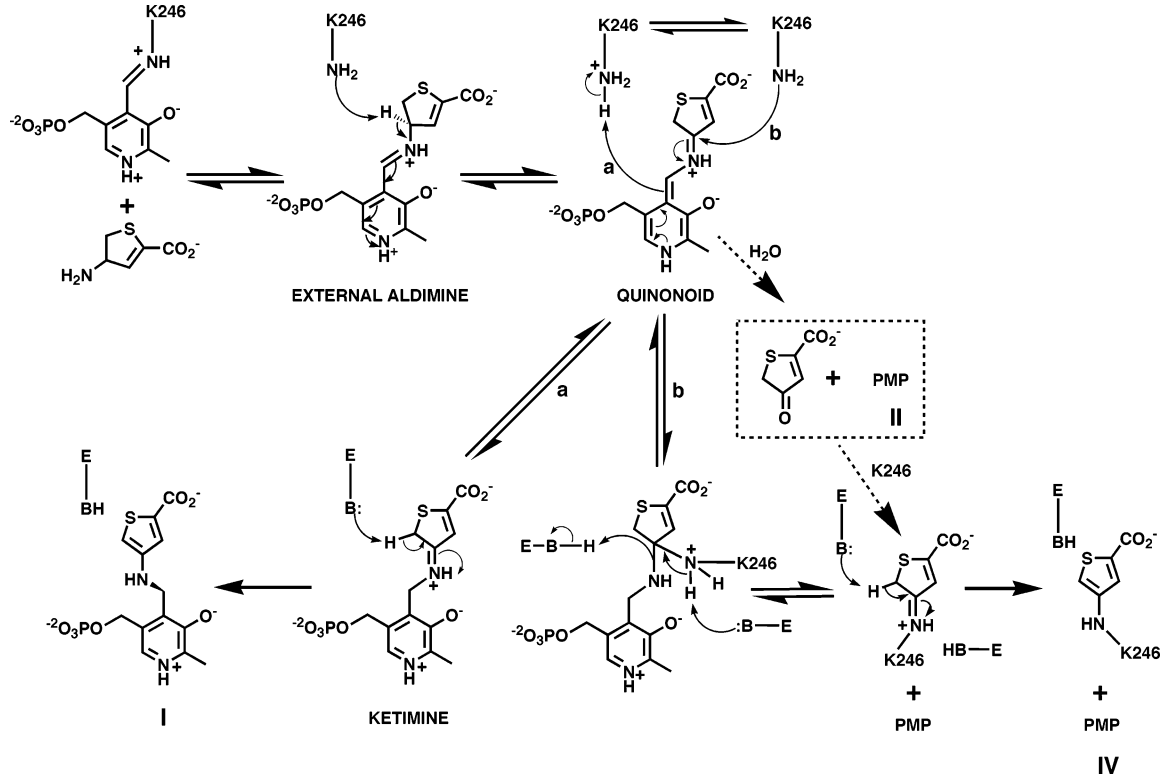

[a] Mechanisms I and II are the same as Scheme 1. Mechanism IV leads to the formation of the K246−SADTA adduct and PMP. a and b indicate the specific steps which lead to mechanisms I and IV, respectively. The enzymatic groups that function as a putative general base or a nucleophile are represented as E−B, while the protonated forms of such groups are shown as E−BH. The identity of such enzymatic groups may or may not be the same in different mechanisms even though they are represented with the same symbol. The dashed frame indicates a possible intermediate proposed in the previous studies that still cannot be eliminated.

and protein are no longer as perfectly aligned as those for the adducts at pH 7.5 or lower in the closer conformation for residues 32−35.

DISCUSSION

Two Different Inhibition Mechanisms for SADTA against L-AspAT. There are a number of mechanisms proposed for the inactivation of PLP-dependent enzymes by SADTA (Scheme 1). In our effort to determine which one occurs, mechanism I was readily confirmed with the identification of the PLP−SADTA adduct in the active site. However, the existence of residual PMP after inhibition (*17*) was interpreted with a different explanation, which is the formation of the K246−SADTA adduct. Therefore, we suggest that SADTA inhibits L-AspAT via two different mechanisms (Scheme 2, mechanisms I and IV).

The first step of the inactivation is the same for both mechanisms, formation of an external aldimine. The amino group of the K246 side chain therefore is freed and serves as a general base to facilitate the formation of quinonoid and/or ketimine intermediates. In the case of inactivation by SADTA leading to derivatization of PLP (mechanism I), the catalytic amino group of K246 could abstract the now sufficiently acidic beta-protons of the dihydro-thiophene ring so that the ketimine can tautomerize, forming a stable PLP−SADTA aromatic adduct irreversibly. Besides K246, Y65* is also close enough to facilitate the tautomerization step. In the case of inactivation by SADTA leading to derivatization of K246, the same ϵ-amino group from K246, which will be increasingly less protonated at higher pH values, can act as a good nucleophile for attack at C4 of the dihydro-thiophene ring in a transaldimination step to form a stable covalent bond with SADTA. This reaction would give a K246−SADTA adduct while producing 1 equiv of PMP (mechanism IV). The K246−SADTA adduct can then form a more stable form as proposed in mechanism IV with the help of another general base. The actual identity of this possible general base is yet to be elucidated. For example, tyrosine 214 and the amino group of the PMP produced might both be close enough to function as a general base for the irreversible step. The possibility of forming the K246−SADTA adduct after going through the old mechanism II (Schemes 1 and 2), however, still cannot be completely eliminated.

From the estimated occupancies, a sharp increase in the occupancy of the K246−SADTA adduct accompanying a correspondingly sharp decrease in the occupancy of the PLP−SADTA adduct occurs between pH 7.5 and 8. This may indicate that the pK_a of the ϵ-amino group of the catalytic lysine is transient in this range, allowing it to act as a nucleophile to attack the C4 atom in the thiophene ring to produce the K246−SADTA adduct and PMP.

Two Binding Orientations of the Inactivator Imply a Complex Conformational Change for the K246−SADTA Adduct. Based on the different binding orientations for the SADTA moieties in either adduct, there could be two different orientations in which SADTA binds to the active site before inhibition (Figures 4 and 7). Each binding orientation correlates with one of the eventual inactivation mechanisms. The PLP−SADTA adduct has the carboxylate

group forming a salt bridge with R374 but not R280*, while K246−SADTA adduct only does so with R280*, not R374. When the inactivator interacts with R374, it will likely bind in an orientation in which the planes of the thiophene ring and PLP are coplanar. When the carboxylate group of SADTA interacts with R280*, the thiophene ring is nearly orthogonal to the PLP plane. However, since both proposed mechanisms involve formation of external aldimine and quinonoid intermediates, such intermediates require the thiophene ring of the inactivator to be coplanar with the PLP ring and the proton at C4 of the thiophene ring to be on the *si*-face of the external aldimine.

We thus propose that the inactivator must initially bind close to the position of the SADTA moiety in the PLP−SADTA adduct. After the formation of the K246−SADTA adduct, the thiophene ring must move from the initial position to the final position we observed in the K246−SADTA adduct. While proposing such a large conformational change, we realize that the carboxylate group of the inactivator has to break free from a rather strong set of interactions, including a salt bridge with R374 and hydrogen bonds from G34 and N183. However, these interactions could be weakened via a specific movement of the flexible loop from residues 32−35 (Figure 6).

Initial Inactivator Binding Preference and Dose Dependence of the Inactivation. Based on the structural models obtained, there may be some binding energy differences between the two orientations of SADTA. When the inhibitor binds in the direction forming a salt bridge with R374, the side chain of N183 and the backbones of G32 and G34 also form hydrogen bonds to facilitate binding of the carboxylate group of the inactivator (Figures 4 and 7). On the other hand, besides the salt bridge, only one hydrogen bond between the inactivator and W130 contributes to the binding direction that leads to the formation of the K246−SADTA adduct. The difference in the number of hydrogen bonds formed between two binding orientations could create a preference for SADTA initially interacting with R374 rather than R280*.

However, a binding conformation in which the carboxylate of the inhibitor interacts with R280* is possible, and SADTA would act as a competitive inhibitor of the inactivation reaction. When the inhibition assays were conducted at a lower concentration of SADTA (1 mM), the enzyme activity could not be completely eliminated despite overnight treatment with inhibitor. This dose dependence of the inactivation may be caused by competition between two binding modes, one leading to inactivation and one not. Eventually, all of the enzyme will be inactivated assuming the second binding mode is reversible.

Structural Comparison among Models at Different pH Values. The crystals formed at different pH values all have similar morphological features, same space group, and very similar cell dimensions. By comparing the structural models obtained at different pH values, the overall structure of the protein changes little and appears only in the open form. The overall structure of L-AspAT is known to have open and closed forms, depending on ligands bound at the active site. When a ligand requires recognition by both binding arginines, R374 and R280* in the active site, the overall conformation of the protein appears as a closed form (*41*−*43*). Since the interactions required to form the closed form do not exist in either individual form of the inactivation complex, all structures obtained in our studies are in the open form.

More importantly, the local structural change that occurs for the loop from residues 32−35 in the active site may allow the movement of the K246−PLP adduct to occur in the final step of mechanism IV. The results suggest that the movement of this region is pH dependent rather than adduct dependent. In the case of SADTA inactivation, the movement of the loop will weaken the binding of SADTA toward R374. First of all, G34 will be too far from the carboxylate group resulting in loss of a hydrogen bond (Figure 6). In addition, the movement of R374 will also put the guanidine group in a less ideal position for forming a salt bridge with the carboxylate group of the inactivator. Therefore, this local structural change could allow the previously discussed movement of the K246−SADTA adduct to occur in the final step of mechanism IV.

Since the occupancies of the two alternate conformations of this loop are not correlated with the occupancies of the two adducts, such movement is likely generic during normal L-AspAT catalysis as well. If this movement also disrupts a salt bridge between the α-carboxylate of the external aldimine and R374 during substrate turnover, it may represent a mechanism for product release. Another noticeable result of this movement is the shortening of the distance between the two guanidinium groups of R374 and R280*. When comparing the structure at pH 6 to that at pH 8, the distance between the two ζ-carbons of the two guanidinium groups is shortened by about 1.1 Å. It is reasonable to think such shortened distance will serve better for binding the 4-carbon substrates (aspartate and oxolacetate) than the 5-carbon ones (glutamate and α-ketoglutarate). The previous pH studies on pig heart aspartate aminotransferase (*28*), which indicated that high pH values favor the binding of the 4-carbon substrate (aspartate) while low pH values favor the binding of the 5-carbon substrate (α-ketoglutarate), are consistent with such reasoning.

CONCLUSIONS

As a mechanism-based inactivator, SADTA inhibits L-AspAT via two possible inactivation mechanisms; the inactivation favors one mechanism or the other depending on the pH values at which the reaction occurs. Two different binding orientations of the inhibitor also contribute to leading the inactivation to different mechanisms. Because each mechanism favors high or low pH values respectively, SADTA is therefore a very potent inactivator of L-AspAT and likely of other similar PLP-dependent enzymes regardless of the pH value. Because it has multiple targets and high potency, SADTA may cause side effects when used as a drug in clinical trials. The differences in dual binding positions and inactivation mechanisms also caused a dose dependent effect as well. Finally, other than transient protonation states of the key catalytic lysine 246, local structural changes in the active site also contribute to the pH dependence of the enzymatic catalysis. Those conformational changes may not be detected when studying pH dependence via steady state kinetics.

ACKNOWLEDGMENT

We thank Dr. Keith Brister and BioCARS staff, especially Dr. Harry Tong, for help and support during data collection

and Drs. Jose Manuel Martinez Caaveiro, Quyen Hoang, and Aaron Moulin for assistance with figure preparation. Use of the Advanced Photon Source (APS) was supported by the U.S. Department of Energy, Basic Energy Sciences, Office of Science, under Contract No. W-31-109-Eng-38. Use of the BioCARS Sector 14 was supported by the National Institutes of Health, National Center for Research Resources, under Grant No. RR07707.

REFERENCES

1. Abeles, R. H., and Maycock, A. L. (1976) Suicide Enzyme Inactivators, *Acc. Chem. Res. 9* (9), 313−319.
2. Rando, R. R. (1974) Chemistry and enzymology of k_{cat} inhibitors, *Science 185* (4148), 320−324.
3. Heifets, L. B. (1994) Antimycobacterial drugs, *Semin. Respir. Infect. 9* (2), 84−103.
4. Adams, J. L., Chen, T.-M., and Brain, W. M. (1985) 4-Amino-4,5-dihydrothiophene-2-carboxlic acid, *J. Org. Chem. 50*, 2730−2736.
5. Burkhart, J. P., Holbert, G. W., and Metcalf, B. W. (1984) Enantiospecific synthesis of (S)-4-amino-4,5-dihydro-2-furancarboxylic acid, a new suicide inhibitor of gaba-transaminase, *Tetrahedron Lett. 25* (46).
6. Schechter, P. J., Hanke, N. F., Grove, J., Huebert, N., and Sjoerdsma, A. (1984) Biochmecal and clinical effects of gamma-vinyl GABA in patients with epilepsy, *Neurology 34* (2), 182−186.
7. Schechter, L. E., Ring, R. H., Beyer, C. E., Hughes, Z. A., Khawajia, X., Malberg, J. E., and Rosenzweig-Lipson, S. (2005) Innovative Approaches for the Development of Antidepressant Drugs: Current and Future Strategies, *NeuroRx 2*, 590−611.
8. Gluck, M. R., Thomas, R. G., Davis, K. L., and Haroutunian, V. (2002) Implications for Altered Glutamate and GABA Metabolism in the Dorsolateral Prefrontal Cortes of Aged Schizophrenic Patients, *Am. J. Psychiatry 159* (7), 1165−1173.
9. Nanavati, S. M., and Silverman, R. B. (1989) Design of potential anticonvulsant agents: Mechanistic classification of GABA aminotransferase inactivators, *J. Med. Chem. 32* (11), 2413−2421.
10. Rando, R. R., and Bangerter, F. W. (1977) Reaction, of the neurotoxin gabaculine with pyridoxal phosphate, *J. Am. Chem. Soc. 99* (15), 5141−5145.
11. Rando, R. R. (1977) Mechanism of the irreversible inhibition of γ-aminobutyric acid-alpha-ketoglutaric acid transaminase by the neurotoxin gabaculine, *Biochemistry 16* (21), 4604−4610.
12. Shah, S., Shen, B., and Brunger, A. (1997) Human ornithine aminotransferase complexed with L-cananline and gabaculine: structural basis for substrate recognition, *Structure 5* (8), 1067−1075.
13. Olson, G. T., Fu, M., Lau, S., Rinehart, K. L., and Silverman, R. B. (1998) An aromatization mechanism of inactivation of γ-aminobutyric acid aminotransferase for the antibiotic L-cycloserine, *J. Am. Chem. Soc. 120*, 2256−2267.
14. Peisach, D., Chipman, D., Van Ophem, P., Manning, J., and Ringe, D. (1998) D-Cycloserine inactivation of D-amino acid aminotransferase leads to a stable noncovalent Protein complex with an aromatic cycloserine-PLP derivative, *J. Am. Chem. Soc. 120*, 2268−2274.
15. Fenn, T. D., Stamper, G. F., Morollo, A. A., and Ringe, D. (2003) A side reaction of Alanine Racemase: Transamination of Cycloserine, *Biochemistry 42*, 5775−5783.
16. Fu, M., Nikolic, D., Breemen, R. B. V., and Silverman, R. B. (1999) Mechanism of inactivation of γ-aminobutyric acid aminotransferase by (S)-4-amino-4,5-dihydro-2-thiophenecarboxylic acid, *J. Am. Chem. Soc. 121*, 7751−7759.
17. Fu, M., and Silverman, R. B. (2004) Inactivation of γ-aminobutyric acid aminotransferase by (S)-4-amino-4,5-dihydro-2-furancarboxylic acid does not proceed by the expected aromatization mechanism, *Bioorg. Med. Chem. Lett. 14*, 203−206.
18. Storici, P., Qiu, J., Schirmer, T., and Silverman, R. B. (2004) Mechanistic crystallography. Mechanism of inactivation of gamma-aminobutyric acid aminotransferase by (1R,3S,4S)-3-amino-4-fluorocyclopentane-1-carboxylic acid as elucidated by crystallography, *Biochemistry 43* (44), 14057−14063.
19. Ross, C. D., and Godfrey, D. A. (1985) Distributions of aspartate aminotransferase and malate dehydrogenase activities in rat retinal layers, *J. Histochem. Cytochem. 33* (7), 624−630.
20. Garcia, R. A. G., and Villegas, J. (1995) Aspartate aminotransferase and glutamate dehydrogenase activities in the squid giant nerve, *J. Neurochem. 64*, 437−442.
21. McKenna, M. C., Stevenson, J. H., Huang, X., and Hopkins, I. B. (2000) Differential distribution of the enzymes glutamate dehydrogenase and aspartate aminotransferase in cortical synaptic mitochondria contributes to metabolic compartmentation in cortical synaptic terminals, *Neurochem. Int. 37* (2−3), 229−241.
22. Daikhin, Y., and Yudkoff, M. (2000) Compartmentation of brain glutamate metabolism in neurons and glia, *J. Nutr. 130* (4S Suppl.), 1026S−1031S.
23. Madl, J. E., and Royer, S. M. (1999) Glutamate in synaptic terminals is reduced by lack of glucose but not hypoxia in rat hippocampal slices, *Neuroscience 94* (2), 417−430.
24. Wood, J., Kurylo, E., and Tsui, D. (1979) Inhibition of aminotransferase enzyme systems by gabaculine, *Neurosci. Lett. 14* (2−3), 327−331.
25. Wada, H., and Snell, E. E. (1962) Enzymatic Transamination of Pyridoxamine II. Crystalline Pyridoxamine-Pyruvate Transaminase, *J. Biol. Chem. 237* (1), 133−137.
26. Wada, H., and Snell, E. E. (1962) Enzymatic Transamination of Pyridoxamine I. With Oxaloaceate and alpha-ketoglutarate, *J. Biol. Chem. 237* (1), 127−132.
27. Kirsch, J. F., Eichele, G., Ford, G. C., Vincent, M. G., Jansonius, J. N., Gehring, H., and Christen, P. (1984) Mechanism of action of aspartate aminotransferase proposed on the basis of its spatial structure, *J. Mol. Biol. 174* (3), 497−525.
28. Kiick, D. M., and Cook, P. F. (1983) pH studies toward the elucidation of the auxiliary catalyst for pig heart aspartate aminotransferase, *Biochemistry 22*, 375−382.
29. Smith, D. L., Almo, S. C., Toney, M. D., and Ringe, D. (1989) 2.8 angstrom resolution crystal structure of an active-site mutant of aspartate aminotransferase from Escherichia coli, *Biochemistry 28* (20), 8161−8167.
30. Kagamiyama, H., and Hayashi, H. (2001) Release of enzyme strain during catalysis reduces the activation energy barrier, *Chem. Rec. 1*, 385−394.
31. Islam, M. M., Goto, M., Miyahara, I., Ikushiro, H., Hirotsu, K., and Hayashi, H. (2005) Binding of C5-dicarboxylic substrate to aspartate aminotransferase: Implications for the conformational change at the transaldimination step, *Biochemistry 44*, 8218−8229.
32. Onuffer, J. J., and Kirsch, J. f. (1995) Redesign of the substrate specificity of Escherichia coli aspartate aminotransferase to that of Escherichia coli tyrosine aminotransferase by homology modeling and site-directed mutagenesis, *Protein Sci. 4*, 1750−1757.
33. Amador, E., and Wacker, W. (1962) Serum Glutamic Oxalacetic Transaminase Activity, *Clin. Chem. 8*, 343.
34. Otwinowski, Z., and Minor, W. *Processing of X-ray diffraction data collected in oscillation mode. Methods in Enzymology*; New York, 1997; Vol. 276, pp 307−326.
35. Miyahara, I., Hirotsu, K., Hayashi, H., and Kagamiyama, H. (1994) X-ray crystallographic study of pyridoxamine 5′-phosphate-type aspartate aminotransferases from Escherichia coli in three forms, *J. Biochem. 116* (5), 1001−1012.
36. Brunger, A. T., Adams, P. D., Clore, G. M., DeLano, W. L., Gros, P., Grosse-Kunstlev, R. W., Jiang, J.-S., Kuszewski, J., Nilges, M., and Pannu, N. S. (1998) Crystallography & NMR system: A new software suite for macromolecular structure determination, *Acta. Crystallogr., Sect. D: Biol. Crystallogr. 54* (Part 5), 905−921.
37. Emsley, P., and Cowtan, K. (2004) Coot: model-building tools for molecular graphics, *Acta Crystallogr., Sect. D: Biol. Crystallogr. 60* (Sp. Iss. 1), 2126−2132.
38. Winn, M. D., Isupov, M. N., and Murshudov, G. N. (2001) Use of TLS parameters to model anisotropic displacements in marcromolecular refinement, *Acta Crystallogr., Sect. D: Biol. Crystallogr. 57* (1), 122−133.
39. Fenn, T. D., Ringe, D., and Petsko, G. A. (2003), *J. Appl. Crystallogr. 36*, 944−947.
40. Pan, Q.-W., Tanase, S., Fukumoto, Y., Nagashima, F., Rhee, S., Rogers, P. H., Argnone, A., and Morino, Y. (1993) Functional Roles of Valine 37 and Glycine 38 in the Mobile Loop of Porcine Cytosolic Aspartate Aminotransferase, *J. Biol. Chem. 268* (33), 24758−24765.

41. Jager, J., Moser, M., Sauder, U., and Jansonius, J. N. (1994) Crystal structures of Escherichia coli aspartate aminotransferase in two conformations, *J. Mol. Biol. 239*, 285−305.
42. Jeffery, C. J., Gloss, L. M., Petsko, G. A., and Ringe, D. (2000) The role of residues outside the active site: structural basis for function of C191 mutants of Escherichia coli aspartate aminotransferase, *Protein Eng. 13* (2), 105−112.
43. Almo, S. C., Smith, D. L., Danishefsky, A. T., and Ringe, D. (1994) The structural basis for the altered substrate specificity of the R292D active site mutant of aspartate aminotransferase from E. coli, *Protein Eng. 7* (3), 405−412.

BI700663N